Tellus (2000), 52B, 1–18
Printed in UK. All rights reserved

Copyright © Munksgaard, 2000
TELLUS
ISSN 0280–6509

Transport of SF_6 and $^{14}CO_2$ in the atmospheric general circulation model ECHAM4

By ERIK KJELLSTRÖM[1]*, JOHANN FEICHTER[2] and GEORG HOFFMAN[3], [1]*Department of Meteorology, Stockholm University, S-10691 Stockholm, Sweden;* [2]*Max-Planck Institute for Meteorology, Bundesstraße 55, D-20146 Hamburg, Germany;* [3]*Laboratoire des Sciences du Climat et de l'Environnement, DSM, Orme des Merisiers, Bat. 703, piece 22 C.E. Saclay, F-91191 Gif-sur-Yvette Cedex, France*

(Manuscript received 23 July 1998; in final form 9 June 1999)

ABSTRACT

Two tracers, SF_6 with sources at the earth's surface and $^{14}CO_2$ with a source in the lower stratosphere, are used to investigate the simulation of global scale transport in an atmospheric general circulation model. The simulated mixing ratios of SF_6 in the troposphere are generally in close agreement to observations revealing a realistic description of the large scale tropospheric transport. The interhemispheric exchange time for SF_6 is calculated to be 0.9 years, indicating a slightly too strong interhemispheric exchange. In the lowermost stratosphere the simulated vertical gradient of SF_6 is in good agreement with observations within the 1st 4 to 5 km above the tropopause indicating that the flux from the troposphere to the lowermost stratosphere is captured by the model. On the other hand, downward transport of $^{14}CO_2$ from the stratosphere into the troposphere is found to be overestimated. From a comparison with observations it is concluded that it is the downward transport in the subtropics that is overestimated, at high latitudes the vertical gradients in the tropopause region are close to observations. Finally, the tracer tests show that the transport into the uppermost two levels, above 20 km, is underestimated as these levels serve as sponge layers and not as layers with a reasonable transport. Consequently, the tracer concentrations in that altitude interval are underestimated, by up to a factor 2.

1. Introduction

In the last few decades an increasing interest in chemical species, man-made and natural, in the atmosphere has developed. The exchange of chemical species within both the troposphere and the stratosphere, and between them (stratosphere–troposphere exchange — STE), is of crucial importance for the chemical balance in these reservoirs. Chemical species of tropospheric origin, like chlorofluorocarbons, methane and sulfur species can, after entering the stratosphere, influence the local chemistry. The stratospheric ozone depletion and the production of sulfate aerosols in the Junge layer around 20 km are two examples (World Meteorological Organization (WMO), 1994; Crutzen, 1976). Downward transport of chemical compounds from the stratosphere to the troposphere, can be of importance for the chemistry in the troposphere (Wang et al., 1998) and maybe also a source of aerosol particles (Song et al., 1996). To study such fluxes of various tracers, atmospheric general circulation models (GCMs) have often been used (Roelofs and Lelieveld, 1995; Kjellström, 1998). However, these models have a coarse resolution, both horizontally and vertically,

* Corresponding author. Present affiliation: Department of Earth, Atmosphere and Planetary Sciences, Massachussetts Institute of Technology, Bldg. 54-1726, Cambridge, MA 02140, USA.
e-mail: erikk@mit.edu.

which can lead to difficulties in calculating STE that occurs on smaller scales.

Previous studies of the transport of chemical tracers in global tracer transport models include both short-lived tracers as ^{222}Rn (Feichter and Crutzen, 1990; Jacob et al., 1997) and long-lived tracers as chlorofluorocarbons (Prather et al., 1987; Waugh et al., 1997). In this study we want to address the question of how accurately a GCM, with its limitations, can simulate STE and also other transport processes like the interhemispheric exchange within the troposphere and the lower stratosphere. The exchange processes at the tropopause are different from upward and downward transport (Holton et al., 1995). Therefore, we investigate the transport of two long-lived tracers; SF_6 which has a surface source, and $^{14}CO_2$ which was emitted into the stratosphere during atmospheric nuclear bomb tests in the 1950s and 1960s.

Recently, SF_6 was proposed as a powerful tracer for evaluating transport in GCMs (Maiss et al., 1996). SF_6 is of anthropogenic origin and emitted at the surface, primarily in the northern hemisphere. An almost quadratic atmospheric increase from 0.03 pptv between the first reported measurement in 1970 to 3.5 pptv in 1996 has been reported by Maiss et al. (1996) and Geller et al. (1997). Chemical reactions of SF_6 with $O(^1D)$ and OH have been reported to proceed very slowly (Ravishankara et al., 1993). They reported reaction rate coefficients of less than 1.8×10^{-14} cm^3 molecules^{-1} s^{-1} for the $O(^1D)$-reaction and less than 5.0×10^{-19} cm^3 molecules^{-1} s^{-1} for the OH-reaction. Also photolysis is very slow with absorption only for wavelengths shorter than 130 nm (DeMore et al., 1997). Ravishankara et al. (1993) concluded that the major destruction of SF_6 is electron attachment in the mesosphere. They estimated the atmospheric lifetime to be 3200 years with a lower limit at 580 years. Since stratospheric sinks are lacking the stratospheric mixing ratios are determined only by the transport time of air from the tropopause. From vertical profiles of SF_6 the age of stratospheric air has been determined (Harnisch et al., 1996; Patra et al., 1997), above 25 km the lag in time, with respect to the troposphere, was found to be 4.5 years for the tropics, 6 years for the midlatitues and 10 years for the Arctic winter vortex. The emission distribution, the steady increase with time, and the stability of SF_6 in the lower atmosphere make SF_6 a suitable tracer for evaluating tracer transport not only in the troposphere but also into the lower stratosphere.

Radioactive ^{14}C was produced during the large nuclear bomb tests mainly in the years 1961–62. ^{14}C also has a natural cosmogenic source, but the excess ^{14}C produced by the bomb tests is a much stronger signal than the natural background production. Excess ^{14}C has been extensively used as tracer for ocean dynamics (Oeschger et al., 1975; Siegenthaler, 1983) and for the carbon exchange between ocean and atmosphere (e.g. Stuiver, 1980; Stuiver et al., 1981; Broecker et al., 1985; Hesshaimer et al., 1994).

Most of the ^{14}C from bomb tests was released in the altitude region between 20 and 30 km, mainly in the northern hemisphere. Therefore, ^{14}C is an attractive tracer to gain information on the stratospheric transport and the STE. By comparing the simulated ^{14}C concentrations with surface observations (Nydal and Lövseth, 1996) of ^{14}C in atmospheric CO_2 (from hereafter the excess radioactive ^{14}C is referred to as $^{14}CO_2$) we will use the $^{14}CO_2$ as a check for the STE as modelled by the ECHAM model. The seasonality of excess $^{14}CO_2$ of about 200–100 per mil observed during the first years after the test stop (1963–1965) in the northern hemisphere is of particular interest since it allows inference on the seasonality of the STE.

2. Model description

In order to simulate the transport of $^{14}CO_2$ and SF_6 we use the atmospheric general circulation model ECHAM4 (Roeckner et al., 1996). The model calculates transport of tracers using a semi-Lagrangian scheme (Rasch and Williamson, 1990) for advection. Convective transport of tracers is calculated with a mass-flux scheme (Tiedtke, 1989) which considers both updraft and downdraft mass fluxes and also entrainment and detrainment. An adjustment closure based on the convective available potential energy is used. Organized entrainment is assumed to depend on buoyancy, and the parameterization of organized detrainment is based on a cloud population hypothesis (Roeckner et al., 1996). The numerical formulation of the convective scheme has been altered in order to

make the convective transport scheme strictly positive (Brinkop and Sausen, 1997).

The ECHAM4 model is run with a spectral triangular truncation at wave number 30 (T30) which corresponds to a Gaussian longitude–latitude grid with a grid spacing of approximately 3.75°. The model uses a hybrid coordinate system with 19 levels from the surface up to 10 hPa. Pressure levels are at approximately 1010, 995, 970, 920, 860, 780, 690, 595, 500, 410, 340, 250, 190, 140, 100, 70, 50, 30 and 10 hPa corresponding to midlayer altitudes of 0.03, 0.08, 0.4, 0.8, 1.4, 2.3, 3.2, 4.3, 5.6, 7.0, 8.6, 10.3, 12.1, 14.0, 16.0, 18.2, 20.6, 23.8 and 31.1 km above the surface. The time step is 30 min. In the experiments the model is run for a 15-year period.

2.1. SF_6 emissions

SF_6 is used in electrical equipment and metal industries and is thought to be of entirely anthropogenic origin in the atmosphere (Maiss and Levin, 1994). The SF_6-production has been increasing almost linearly since 1970 (Maiss et al., 1996). The history of the SF_6-emission to the atmosphere has been estimated from the observed atmospheric increase (Maiss and Levin, 1994). In this experiment we use the same method for calculating SF_6 emissions as in the TransCom2 experiment (Denning et al., 1999). The expression from Levin and Hesshaimer (1996):

$$E = 0.2133(t - 1990) + 4.913, \quad (1)$$

where E is the emission in Gg SF_6 per year and t is the time in years AD is used in this work. The horizontal distribution of the SF_6 emissions, which is calculated from the electric power usage per country (UN Energy Statistic Yearbook, 1992), was provided by Martin Heimann (personal communication). About 95% of the emission is located in the northern hemisphere (Fig. 1). The SF_6 experiment is started with zero mixing ratios in October 1970.

2.2. Initial distribution and sinks of $^{14}CO_2$

On the basis of measurements done by the US Atomic Energy Commission in the period from 1955 to 1970 and published in reports of the Health and Safety Laboratory (Telegadas, 1971; Telegadas et al., 1972), Johnston (1989) established a $^{14}CO_2$ data set particularly adapted as initial condition for testing atmospheric transport models. The initial $^{14}CO_2$ data are zonally uniform and have a latitudinal resolution of 10°. The vertical resolution is 1 km between the surface and

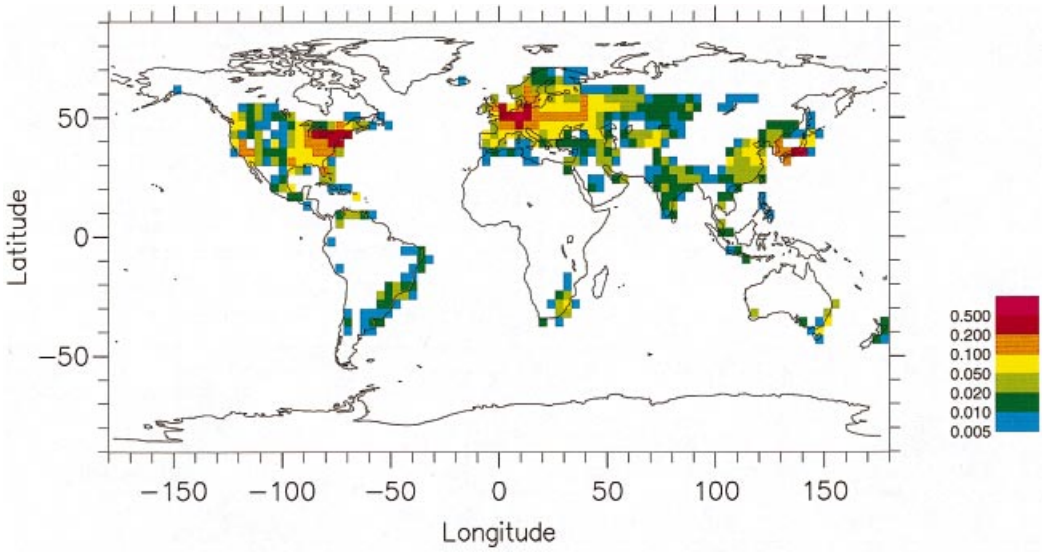

Fig. 1. Horizontal distribution of SF_6 emissions. The emissions are representative for January 1980. Unit: mg SF_6 m^{-2} yr^{-1}.

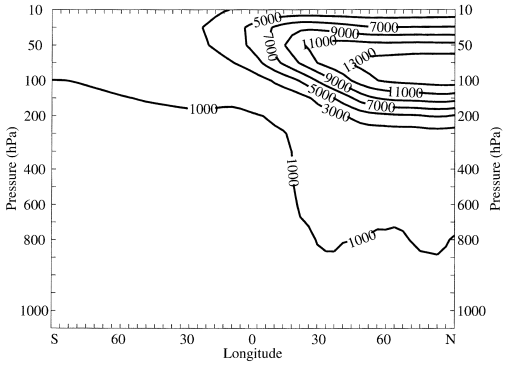

Fig. 2. Initial distribution of excess $^{14}CO_2$. Unit: per mil excess relative to the US National Institute of Standards and Technology.

50 km height. The data describe the global distribution of excess $^{14}CO_2$ in October 1963 well after the Test Ban Treaty in 1962. At the end of 1963 the original bomb signal was already well mixed zonally. The initial data were linearly interpolated on the ECHAM4 grid, see Fig. 2.

The sink of atmospheric $^{14}CO_2$ is uptake at the earth's surface, in vegetation and in sea surface water. We follow the approach by Hesshaimer et al. (1994) by introducing three boxes representing the terrestrial biosphere and a constant sink representing the oceans. The first biospheric box represents fine roots, twigs and leaves (with a total carbon content of 105 Tg C), the second big roots, stems and branches (675 Tg C) and the third slowly decomposing material from the other two biospheric boxes (1420 Tg C). The carbon in the three biospheric boxes is decomposed exponentially with a turn-over time of 3, 27 and 375 years respectively. Box 1 and 2 are directly coupled to the atmosphere with an input from the atmosphere adding up to 60 Tg C yr^{-1}, corresponding to the net primary production. Box 3 gets its carbon input equally distributed from box 1 and 2, and ventilates into the atmosphere. For the flux of CO_2 between the atmosphere and the oceans a gross flux of 60 Tg C yr^{-1} is assumed. The actual $^{14}CO_2$ flux between the different reservoirs is calculated as the flux of CO_2 times the ratio between ^{14}C and ^{12}C in the different reservoirs. Only the long-time variations are considered by this sink description, seasonal changes in the sinks are not accounted for.

3. Results and discussion

3.1. Long-term trends

With linearly increasing emissions, the global average mixing ratio of SF_6 in the model follows a quadratic increase with time given by

$$\psi(t) = 0.0042t^2 + 0.0228t - 0.0211, \quad (2)$$

where $\psi(t)$ is the global average mixing ratio in pptv and t is the time (years) after 1970, Fig. 3.

A quadratic increase with time of SF_6 concentrations has been observed by Maiss et al. (1996) and Geller et al. (1997) for the time period 1978–1996. A comparison of the simulated increase to the trend derived from the observations by Maiss et al. (1996) shows that the model lags behind since it starts with zero concentrations in 1970 (Fig. 3). Also, the simulated trend shows a faster increase than the trend derived by Maiss et al. (1996) since our emissions increase at a slightly higher rate. Because of these two differences the model results cannot directly be compared with observed concentrations. The difference between the simulated and observed mixing ratios at a certain time varies between 0.1 and 0.15 pptv during the time period 1973 to 1983. In order to compare model simulated and observed mixing ratios during that period the average difference during those years, 0.13 pptv, is added to the model simulated mixing ratios.

Seen over a long time the $^{14}CO_2$-content in the

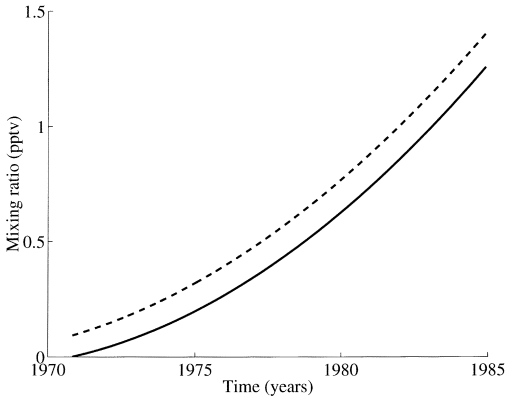

Fig. 3. Trend in global average SF_6 mixing ratio. Simulated trend as described by eq. (2) (full line) and observed trend according to Maiss et al. (1996) (dashed line).

model domain decreases exponentially with time with an e-folding time of seven years as a global average (Fig. 4). Initially the simulated $^{14}CO_2$ increases in the troposphere due to the downward transport from the stratosphere. However, already after one year of the simulation, the tropospheric $^{14}CO_2$-content also decreases when the surface sinks have become more important than the input from the stratosphere.

3.2. Simulated geographical distributions

The simulated distribution of SF_6 shows higher mixing ratios in the northern hemisphere than in the southern hemisphere, see Fig. 5a. Elevated mixing ratios are found in, or downstream of, the industrialized regions. In the southern hemisphere, where sources are almost absent, the predicted mixing ratios are lower and more uniform than in the northern hemisphere. Above the boundary layer the distribution is zonally symmetric except at mid and high northern latitudes (north of 40°N) where the mixing ratios are slightly higher over the Eurasian continent than over North America and Greenland (Fig. 5b). This difference is caused by the distribution of the emissions with the European sources being located further to the north than the North American sources. At higher tropospheric levels this difference decreases and above the tropopause level the annual mean is more zonally symmetric also at these latitudes. In the stratosphere the concentration decreases with height due to the slow mixing into these high levels. The stratospheric mixing ratios decline from the equator towards the poles in both hemispheres with the lowest mixing ratios in the northern hemisphere (Fig. 5c).

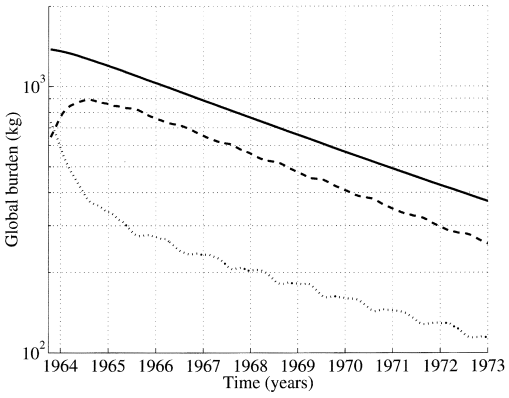

Fig. 4. Trend in global (full line), tropospheric (dashed line) and stratospheric (dotted line) $^{14}CO_2$ burden.

Also for $^{14}CO_2$ the simulated distribution is zonally symmetric in the stratosphere on an annual mean basis (not shown). However, on shorter timescales (weeks or months), large-scale features like the planetary waves appear in the simulated distributions (this is also the case for SF_6). Unlike for SF_6, the mixing ratios in the stratosphere are lowest at low latitudes revealing upward transport of $^{14}CO_2$-poor tropospheric air at these latitudes. The tropospheric mixing ratios are zonally uniform in general (Fig. 6). However, certain features are still present. First, higher mixing ratios are calculated in the northern hemisphere than in the southern hemisphere due to the initial distribution of the stratospheric $^{14}CO_2$. Further, the mixing ratios are highest in the subtropics of the northern hemisphere troposphere where the combination of high stratospheric $^{14}CO_2$-content, isentropic mixing of stratospheric air into the troposphere and downward motion is an effective source of tropospheric $^{14}CO_2$. Local maxima are also seen in the subtropics of the southern hemisphere but not as strong as in the northern hemisphere since the stratospheric content at these latitudes is smaller than at the corresponding northern latitudes.

3.3. Interhemispheric exchange

The interhemispheric exchange time (τ_{ex}), which is a measure of the exchange between the hemispheres, may be defined by

$$\tau_{ex} = (M_{NH} - M_{SH})/F_{NH-SH}, \quad (3)$$

where M_{NH} and M_{SH} are the tracer mass in the respective hemispheres, and F_{NH-SH} is the net flux of the tracer from the northern to the southern hemisphere (Prather et al., 1987).

We calculate an interhemispheric exchange time of 0.9 years which is slightly lower than the 1.1 years calculated in the 2D-model by Levin and Hesshaimer (1996) and the 3D-model by Jacob et al. (1987) using ^{85}Kr. The simulated transport between the hemispheres is most efficient at the solstices when the intertropical convergence zone (ITCZ) is located at its northern or southern extreme (Fig. 7). Levin and Hesshaimer (1996) calculated the monthly varying interhemispheric

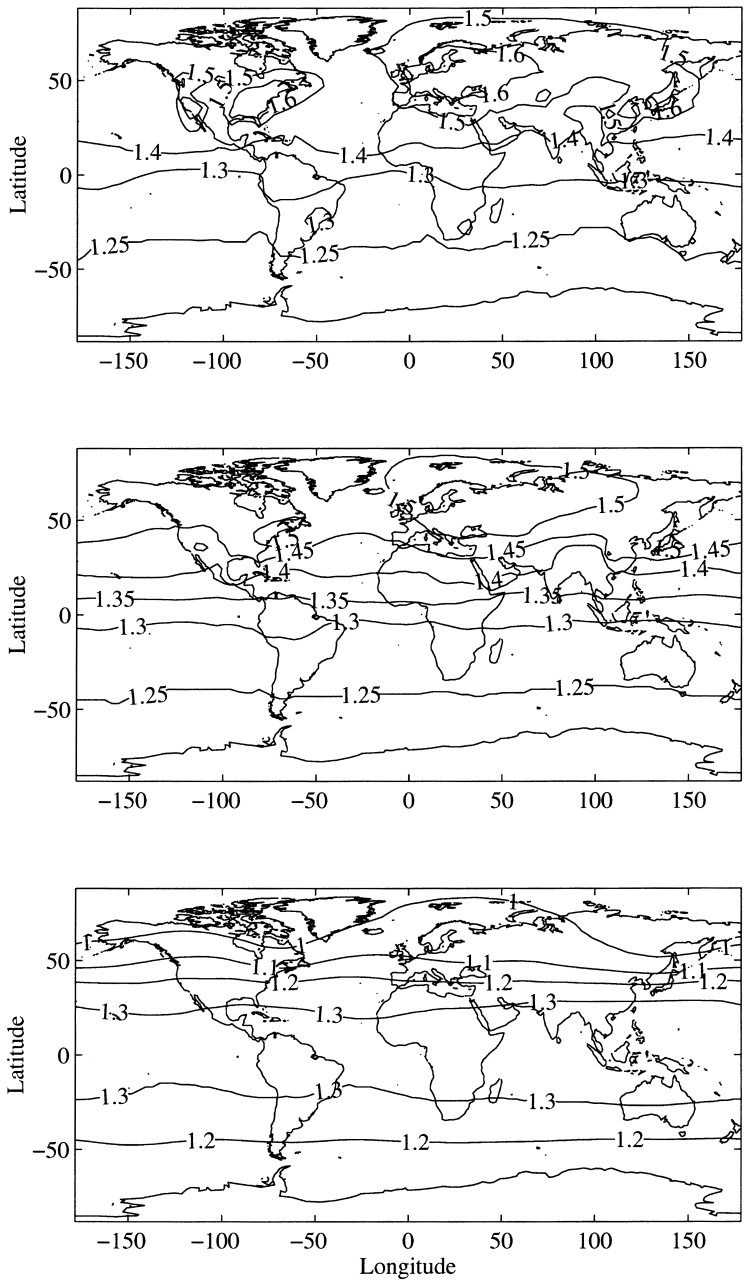

Fig. 5. Annual average distribution of SF_6 from year 15 (corresponding to 1984) in the simulations. Lowest model level (top panel), 850 hPa (middle panel) and 100 hPa (lower panel). Unit: pptv.

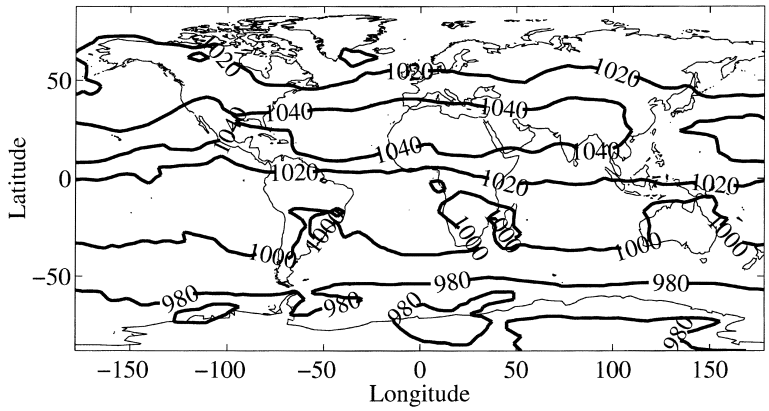

Fig. 6. Distribution of $^{14}CO_2$ at 700 hPa from January of the fourth year of the simulations (corresponding to 1966). Unit: per mil excess relative to the US National Institute of Standards and Technology.

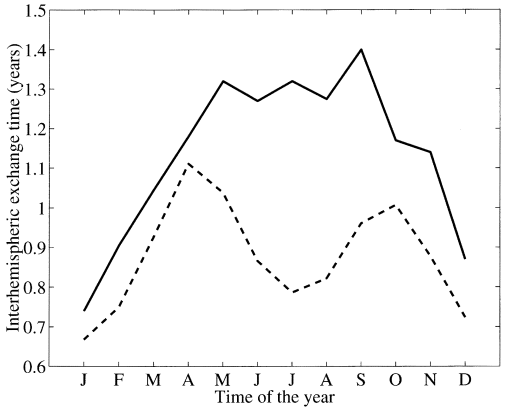

Fig. 7. Seasonal variation of the interhemispheric exchange time as calculated in the model (dashed line). The corresponding values from Levin and Hesshaimer (1996) are included as a comparison (full line).

exchange time and found a slightly stronger seasonal cycle than here, but unlike our results, they found no minimum in the interhemispheric exchange time in the northern hemisphere summer (Fig. 7). This lack of a summer minimum is the main reason for why their annual average interhemispheric exchange time is higher than ours, in this work a stronger interhemispheric exchange is predicted also during northern hemisphere summer.

The simulated interhemispheric exchange time is considerably shorter than the 1.3–1.7 years that have been estimated with two-box models using the observed difference in SF_6 concentration between the two hemispheres (Maiss et al., 1996; Levin and Hesshaimer, 1996 and Geller et al., 1997). In these studies the difference between the hemispheres was derived primarily from observations at the surface. As pointed out by Jacob et al. (1987) and Levin and Hesshaimer (1996); using the high concentrations of respectively ^{85}Kr and SF_6 in the northern hemisphere boundary layer as representative for the northern hemisphere will lead to a too strong interhemispheric gradient and thereby to relatively long interhemispheric exchange times in simple box-models. 2- and 3-dimensional models take into account also the vertical distribution of the tracer, thereby reducing the interhemispheric gradient (Fig. 8) and calculating a shorter interhemispheric exchange time. Nevertheless, compared with observations the model simulated latitudinal distribution shows a slightly weaker latitudinal gradient implying a somewhat too strong interhemispheric transport.

Maiss and Brenninkmeijer (1998) derive expressions for hemispheric trends of SF_6. Comparing their hemispheric trends show that the difference between the northern and southern hemispheres increase with 0.01 pptv yr^{-1} during the time period 1970 to 1985. In this study an increase of 0.008 pptv yr^{-1} is calculated. The slower increase of the difference between the hemispheres strengthens the notion of an overestimated interhemispheric exchange.

3.4. Seasonal variations

The seasonal variations of SF_6 depend only on the dynamics and transport of the model since

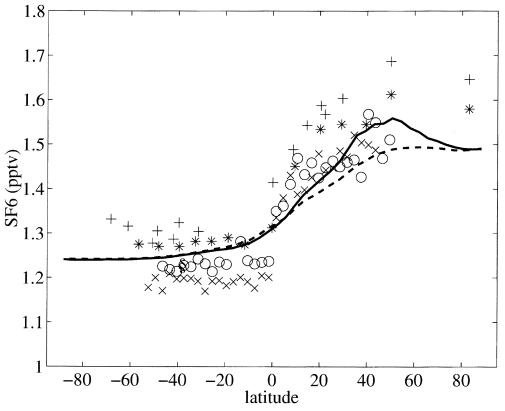

Fig. 8. Latitudinal distribution of SF_6. Simulated zonal means; lowest model level (full line) and 850 hPa (dashed line). Oceanic shipboard measurements from Maiss et al. (1996) and Geller et al. (1997) are plotted as: (+) the Atlantic in November 1990, (*) the Atlantic in November 1993, (×) the Pacific Ocean in January–February 1994 and (○) the Atlantic in October–November 1994. All observational data have been scaled to July 1984 according to Geller et al. (1997). The corresponding observation at Cape Grim is shown for comparison (§).

there are no seasonal variations in the emissions. In the boundary layer at high northern latitudes the simulated mixing ratios are higher in winter than in summer (not shown). The higher ratios during winter are due to the more stable boundary layers and also due to the northward transport from the source regions into the Arctic region during this season. The amplitude of this high latitude seasonal cycle is almost 5% of the detrended annual mean (i.e. the long-term trend discussed in Subsection 3.1 has been removed). The opposite seasonal variation can be seen in the free troposphere where mixing ratios are higher during summer due to convection. The strongest seasonal cycle of SF_6 in the troposphere, with an amplitude of more than 10%, is simulated in the boundary layer of the equatorial region due to the movement of the ITCZ. In this region high mixing ratios are calculated in the northern hemisphere winter when the ITCZ is displaced to the south. At mid and high latitudes in the southern hemisphere, where sources are almost absent, the amplitude of the seasonal variations is less than 1%.

Almost 10 years of high temporal resolution data from Neumayer in Antarctica (71°S, 8°W), provide a possibility of studying the seasonal behaviour of SF_6 at a remote site. The model captures the main features of the seasonal cycle — the low mixing ratios in austral summer and the high mixing ratios in spring (Fig. 9). The seasonal cycle at these high latitudes lags with 6 to 7 months compared with the equatorial region. This lag corresponds to the simulated transport time of air from the equator to the South Pole region. The amplitude of the seasonal cycle at Neumayer is underestimated by almost a factor 2, a feature also noted by Levin and Hesshaimer (1996) with their 2D-model. Based on observations of ^7Be, which is primarily of stratospheric origin, at Neumayer they claim that a too weak downward transport of stratospheric air may contribute to their underestimate. Downward transport of stratospheric air would give lower mixing ratios of SF_6 but also higher mixing ratios of $^{14}CO_2$ at the surface. We calculate both $^{14}CO_2$ and SF_6 to be highest (lowest) in austral spring (summer). This coherence, between $^{14}CO_2$ and SF_6, indicates that the relatively low simulated SF_6 mixing ratios in summer does not have to do with downward mixing of stratospheric air which is low in SF_6. Contributing to the too weak simulated seasonal cycle at Neumayer could be a poor representation of the seasonal cycle of either the interhemispheric exchange (as discussed in Subsection 3.3) or the transport into mid and high southern latitudes.

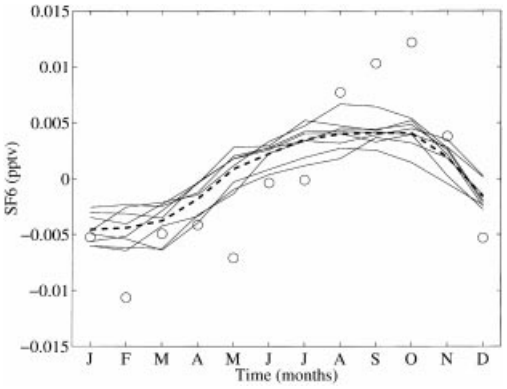

Fig. 9. Seasonal cycle of SF_6 at Neumayer, Antarctica (71°S, 8°W). The seasonal deviation from the average of the last 8 years of the simulations is drawn as a dashed line. The interannual variation is represented as the seasonal deviation from the average for each year (full lines). Observations from 1988 to 1993 (except February 1991 to February 1992) are from Maiss et al. (1996) (○).

From the Neumayer data alone it is impossible to judge which is the most likely shortcoming in the model.

3.5. *Comparison with SF_6 observations — upward transport from the troposphere*

Simulated SF_6-mixing ratios are compared with the AIRSTREAM observations (Leifer, 1992) (Fig. 10). These observations cover a latitudinal region between 75°N and 51°S over the Pacific Ocean and North America and a height range from below the tropopause up to about 20 km. The agreement between model and observations in the lower stratosphere is within 10% up to 4 or 5 km above the tropopause both in the tropics and at mid and high latitudes. Above that level the simulated mixing ratios drop off faster than the observations with increasing altitude. At mid and high latitudes (polewards of 30°) the calculated mixing ratios are systematically about 30% lower than the observations at 10 km above the tropopause. In the tropics (equatorwards of 15°) the underestimate is about 20% at 5 km above the tropopause.

At higher stratospheric levels the underestimate is even stronger. Compared with the observed SF_6-profiles shown in Fig. 11, the model underestimates the SF_6-content in the upper model domain by up to a factor of 2 at 30 km altitude. The relatively better agreement between the 2 soundings from northern Sweden in January and February is explained by the fact that the observations were made inside the Arctic polar vortex where air with very low SF_6 mixing ratios is sinking from higher levels. At lower altitudes a

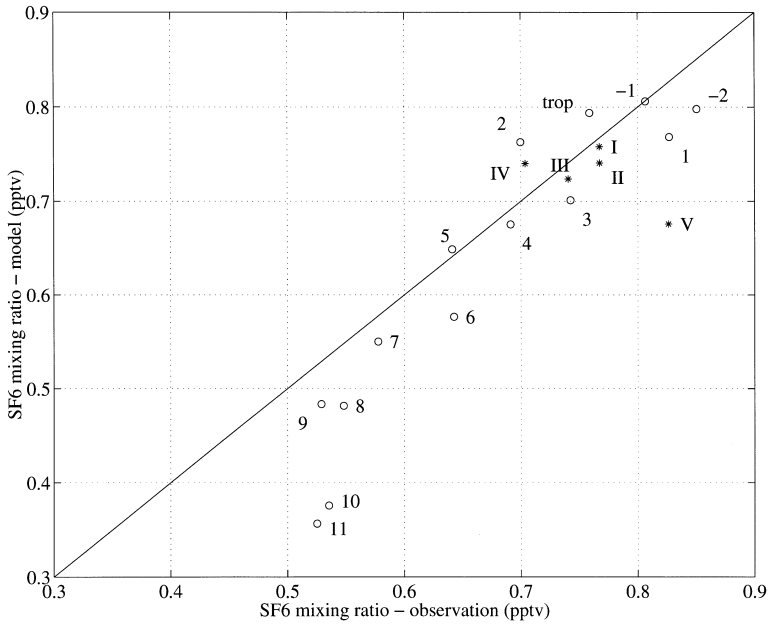

Fig. 10. Comparison between observed SF_6 mixing ratios from project AIRSTREAM (Leifer et al., 1992) and corresponding simulated mixing ratios. The observations, which include 860 samples, cover the time period 1973–1983. The original data have been scaled depending on which laboratory that made the analysis, the scaling factors are: 1.18-HASL, 1.52-WSU and 1.76-OGC (Ingeborg Levin, personal communication). All the data, both model and observations, have been scaled to 1 January 1980 according to the Maiss et al. (1996) observed trend. 0.13 pptv has then been added to the simulated data (see text). The figure shows model versus observations where all data have been averaged and binned in altitude intervals of 1 km. Data representing the tropics (equatorwards of 15° latitude) are denoted with asteriscs and data representing high and mid latitudes (polewards of 30°) with circles. The numbers indicate the altitude relative to the calculated or observed tropopause height in km. The tropopause height is defined as the lowest level at which the temperature lapse rate is 2 K km^{-1} and the average lapse rate between this level and any upper level within 2 km does not exceed 2 K km^{-1} (WMO, 1986).

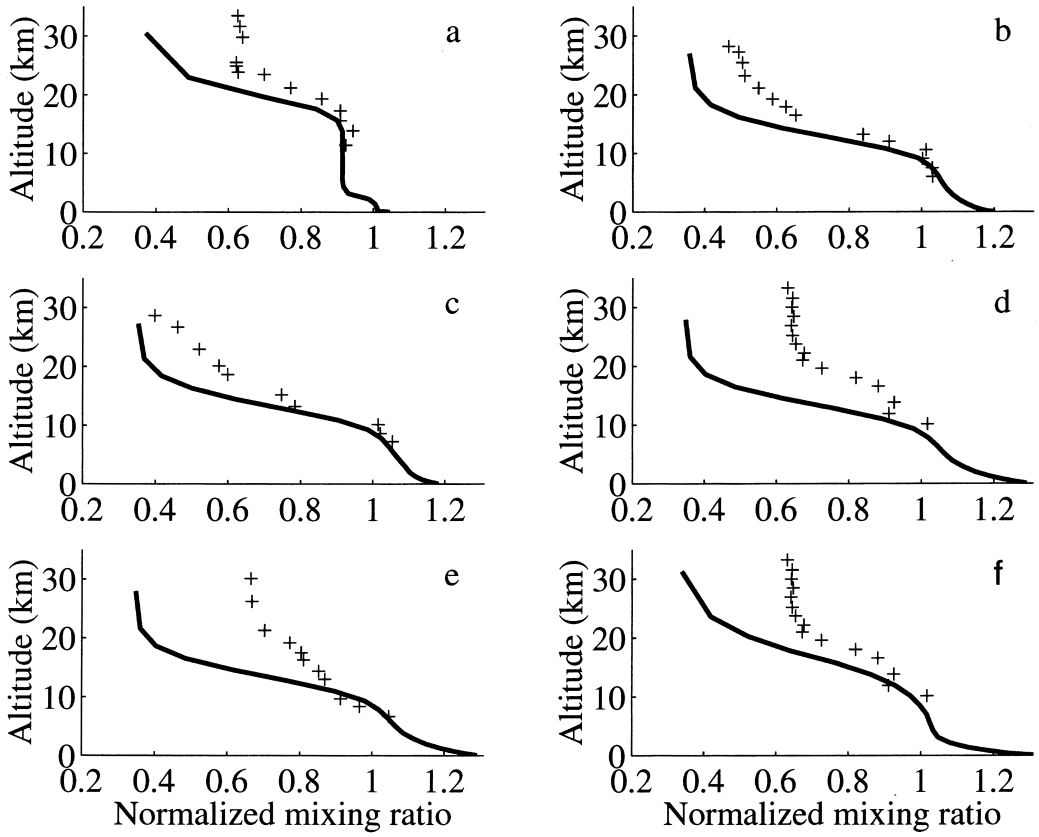

Fig. 11. Vertical distributions of SF_6. Observed profiles from balloon soundings (Harnisch et al., 1996) (+) and simulated monthly means (full line). The profiles have been normalized by the average northern hemisphere tropospheric SF_6 mixing ratio, taken from the trend derived by Geller et al. (1996), at the time of the sounding. The profiles are from (a) Hyderabad (India) in March, (b–e) Esrange (Sweden) in January (b), February (c), March (d), March — outside the polar vortex (e) and (f) Aire (France) in October.

qualitatively good agreement between model and observations is seen for all the soundings where the lowermost observation in each sounding is from the troposphere. There are two reasons for the unrealistic transport in the uppermost model layers: First, a damping of waves in the uppermost model domain is included in the parameterization of horizontal diffusion to avoid reflection of waves at the upper boundary (Roeckner et al., 1996). Second, no transport can occur across the upper boundary of the model in contrast to the real atmosphere in which vertical transport extends into higher levels.

The age of a stratospheric air parcel can be defined as its mean transit time from the tropical tropopause (Hall and Plumb, 1994). Since the concentration of SF_6 in the troposphere exhibits a relatively slow and steady increase the stratospheric SF_6 concentration is a function only of the age of stratospheric air (Hall and Plumb, 1994). Fig. 12 shows the distribution of time until the zonally averaged simulated mixing ratios of SF_6 reach 0.3 pptv compared to the time when this level was first reached in the boundary layer of the source regions. About 1.5 years elapse between the time when the mixing ratios first reach this level in the source regions until the same mixing ratios are simulated at the tropical tropopause. This result is almost identical to what Hall and Plumb (1994) found for a passive tracer with a northern mid latitude source. It is also consistent with the 0.8 years calculated by Waugh et al.

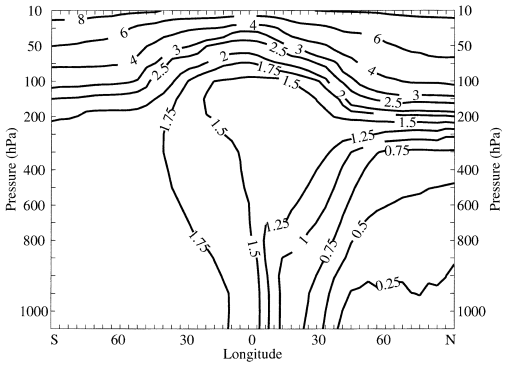

Fig. 12. Zonally averaged time until the calculated mixing ratio of SF_6 reached 0.3 pptv compared to the time when this level was first reached in the boundary layer of the source regions. Unit: years.

(1997) since they compared the time at the tropical tropopause with the global averaged trend at the surface derived by Geller et al. (1997). Above the tropical tropopause the calculated age of stratospheric air increases with altitude in a similar way as found by Hall and Plumb (1994) and by Waugh et al. (1997). At higher altitudes the problem with the upper boundary, as discussed in the previous section, leads to lag times that are about twice as long as in their modelling studies and as observed by Harnisch et al. (1996).

The model simulates lower ages in the stratosphere of the southern hemisphere than in the northern hemisphere indicating that the poleward transport of air is stronger in the southern hemisphere. This result is consistent with results from Rosenlof and Holton (1993) when they calculate the horizontal flux of air across an idealized tropopause break between 100 and 200 hPa at 30° latitude. They found this horizontal flux to be almost twice as large in the southern hemisphere as in the northern hemisphere during December, January and February. However, our results are in contrast to the observed age distributions derived from SF_6 observations by Elkins et al. (1996) and modelled by Waugh et al. (1997). The difference can be illustrated by the interhemispheric difference in October for which Waugh et al. (1997) compare their results to the measurements from Elkins et al. (1996). At 19.8 km they calculate a latitudinal gradient in age of about 1 year between the equator and 30°N and almost 2 years between the equator and 30°S. This age distribution is in fair agreement with the measurements by Elkins et al. (1996), though the latitudinal gradients are somewhat too small (Waugh et al., 1997). The corresponding gradients in our simulation are about 1.5 and 0.5 years in the respective hemispheres. The small gradient in the southern hemisphere, which is obtained in all seasons, implies that our model has too fast poleward transport in the southern hemisphere. This too strong meridional transport is associated with the too strong meridional temperature gradient, between the tropics and the polar region in the model, which enhances the baroclinicity and thereby the horizontal mixing (Roeckner et al., 1996). At high northern latitudes we find a seasonal cycle with a larger latitudinal gradient in age during winter and spring than in summer which could be attributed to the slower mixing into the polar vortex.

3.6. Comparison with $^{14}CO_2$ observations — downward transport from the stratosphere

Observed vertical profiles of $^{14}CO_2$ from Johnston (1989) are compared with simulated zonal mean profiles at 70°N, 30°N, 9°N, and 42°S, Figs. 13, 14. The observations were carried out initially 4, and later 2 × per year during the time period 1963–1970. As for SF_6, the agreement between calculated and observed mixing ratios in the stratosphere is best in the 1st 4 to 5 km above the tropopause (corresponding to about 20 km in the tropics and 15 km in the mid-latitudes). The best agreement in the lower stratosphere and in the troposphere is found at 70°N while at lower latitudes concentrations in this altitude region are overestimated. This overestimation together with an underestimation at the height of the peak levels (Fig. 13) indicate a too rapid downward transport of stratospheric $^{14}CO_2$. Further, the underestimated concentrations above the altitude of the peak levels suggest that the upward transport to the uppermost model layers is too weak.

From the stratospheric $^{14}CO_2$-content reported by Telegadas (1971), Johnston (1989) estimated the e-folding time of the global inventory of stratospheric $^{14}CO_2$ to be 2.3 years from January 1963 until October 1964, and 5.7 years between January 1965 and July 1966. The difference between the two time periods reflects the rapid removal of $^{14}CO_2$ from the lower stratosphere at the

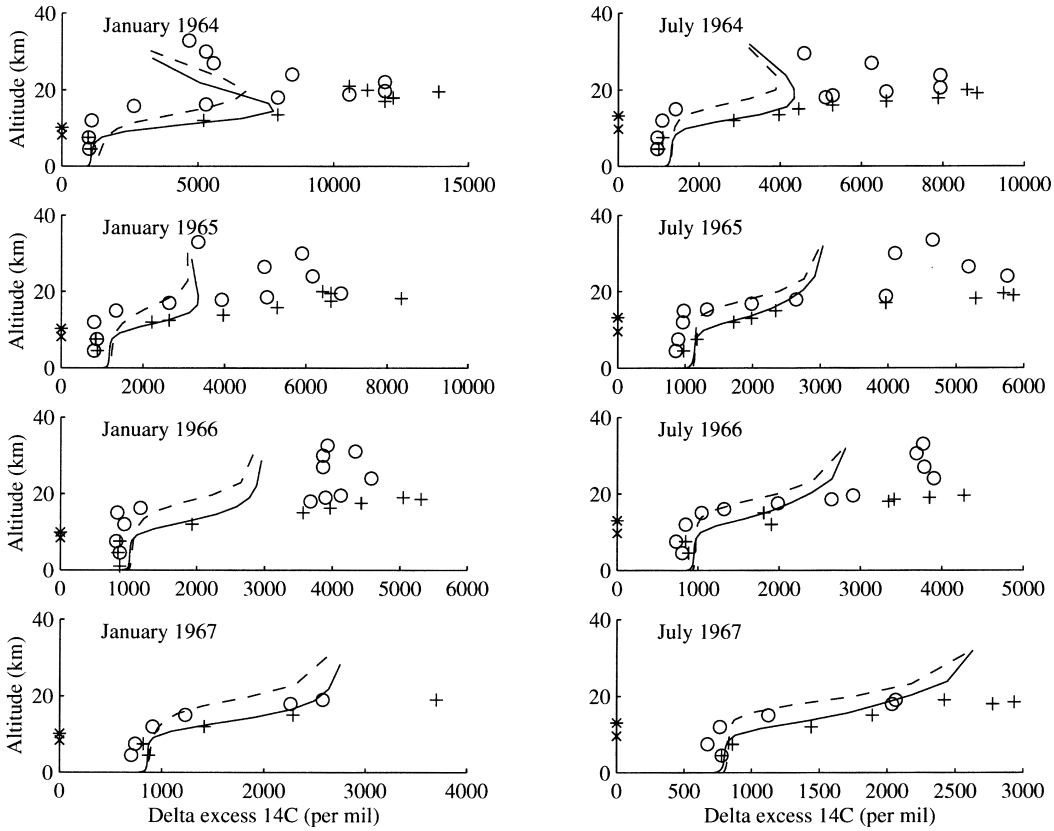

Fig. 13. Observed vertical profiles of $^{14}CO_2$ at 70°N (+) and 30°N (○) from Johnston, 1989. Corresponding simulated profiles from the model are shown as a solid line at 70°N and a dashed line at 30°N. The model tropopause level is indicated as × (70°N) and * (30°N) on the altitude axis.

beginning of the integration. At higher altitudes the $^{14}CO_2$ remained longer and it is that part of the stratospheric $^{14}CO_2$ content which determines the lifetime in the latter period (Johnston, 1989). We calculate corresponding lifetimes of 1.3 years for the period between October 1963 and October 1964 and 5.2 years for the latter period. The rapid decrease of stratospheric $^{14}CO_2$ at the beginning of the simulation indicates a too strong flux to the troposphere. One possible reason for this too strong downward flux of stratospheric air could be the coarse vertical resolution in the model. In order to investigate the influence of vertical resolution we have compared our results with a version of the ECHAM4 model that has 39 vertical levels between the surface and 10 hPa (model version L39). In the tropopause region L39 has a vertical resolution of 0.75–1 km compared to 1.5–2 km in our model (L19). In L39, the initial $^{14}CO_2$-content also decreases too fast with an e-folding time of 1.3 years for the fist period (Land, 1999) similar to L19. This too fast decrease also in L39 indicates that the vertical resolution is not the main problem unless an even higher vertical resolution is required. Nevertheless, during the first months of the simulation L39 performs better compared to the observations implying that the vertical resolution has some impact on the simulations. The rather good agreement between our model and the observations in the latter period does not imply that the calculated transport to the troposphere is better, it merely reflects the combination of a fast downward transport from the lowermost stratosphere and a slow vertical transport in the uppermost model domain as discussed in the previous section.

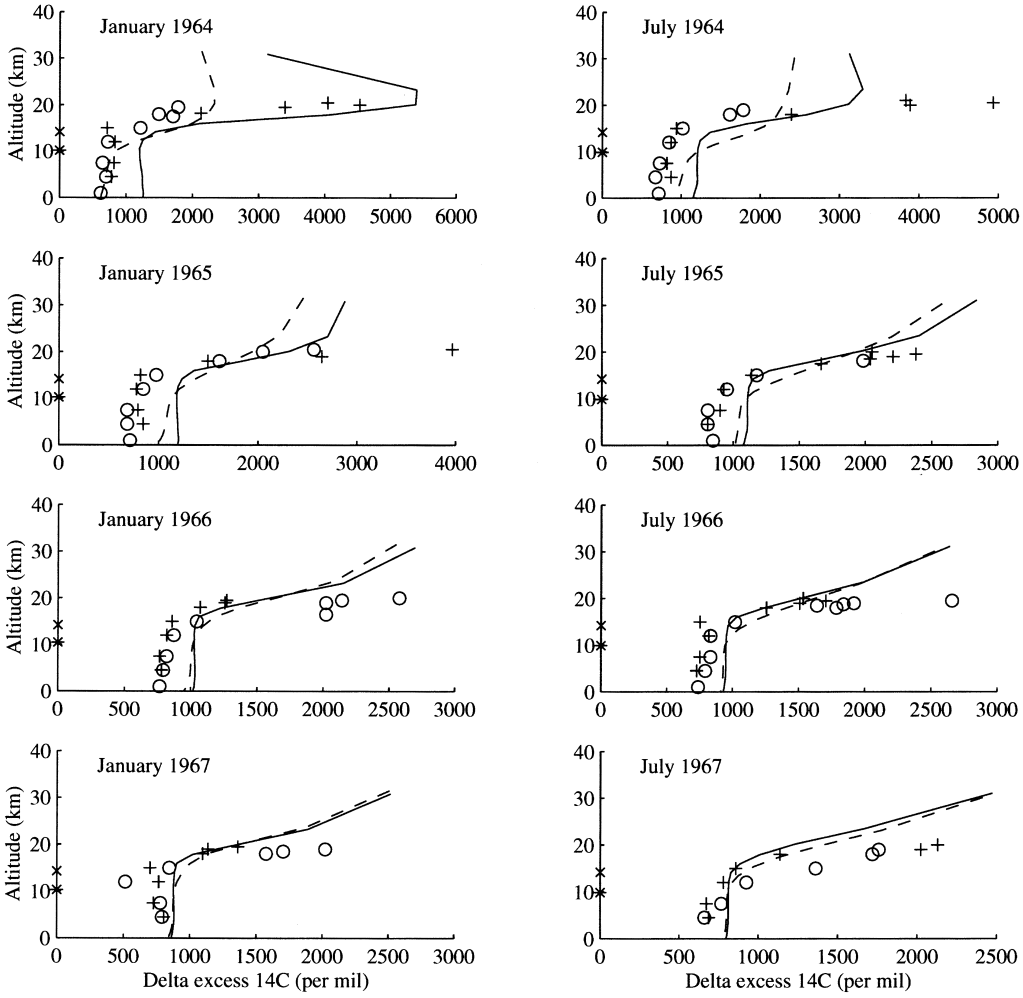

Fig. 14. Observed vertical profiles of $^{14}CO_2$ at 9°N (+) and 42°S (○) from Johnston, 1989. Corresponding simulated profiles from the model are shown as a solid line at 9°N and a dashed line at 42°S. The model tropopause level is indicated as × (9°N) and * (42°S) on the altitude axis.

Compared with the observed profiles from Johnston (1989) the simulated mixing ratios of $^{14}CO_2$ in the lowermost stratosphere become too high within a few months after the start of the simulation (Figs. 13, 14). This pattern, which is common to all latitudes except 70°N where the agreement between observations and model results is good throughout the simulations, indicates that the downward transport of $^{14}CO_2$ is overestimated at lower latitudes. Both at 30°N and especially at 42°S, also the tropospheric mixing ratios in the first months of the simulations are overestimated, which implies a too strong downward flux from the stratosphere. Further, the overestimation in the southern hemisphere troposphere and lowermost stratosphere (Fig. 14) suggests that the interhemispheric transport is too strong. A too strong downward tracer flux is consistent with calculations of air mass flux across the tropopause in a previous model version ECHAM3 by Grewe and Dameris (1996): they found that the model overestimates the downward flux at 30°N and 40°S with a factor of approximately 1.5 to 2. The better agreement to observations that we find at higher

latitudes (70°N) is consistent with the results by Kentrachos et al. (1999) who use the same model as in this study applied to a specific synoptic situation over Europe. They conclude that the model is able to predict intrusions of stratospheric O_3 into the troposphere in a realistic way. A possible reason for the too strong downward transport at lower latitudes could be insufficient horizontal resolution. Siegmund et al. (1996) use analysed meteorological data to investigate the STE. In going from a horizontal resolution of 0.5° to 3.75° they find that the maximum downward flux close to 30°N increase with almost a factor 3. At mid and high latitudes, on the other hand, they find the average cross tropospheric flux to be much less sensitive to the horizontal resolution. Also contributing to a too strong downward flux could be a too strong horizontal isentropic mixing (see last paragraph of Subsection 3.5) followed by downward motion in the subtropics.

At the surface of the northern hemisphere the model predicts a rapid increase in $^{14}CO_2$ during the first year of the simulation. Fig. 15 shows the time when the maximum $^{14}CO_2$ concentration at the model level closest to the surface is reached. The fastest downward transport of $^{14}CO_2$ is predicted in the subtropics of the northern hemisphere where the maximum at the surface is reached within 4 to 6 months from the start of the simulations. Also the northern hemisphere tropics experience the maximum at an early stage due to northerly winds during the winter when the peak first reaches the surface, later on the ITCZ moves northwards passing these regions. Within 1 year the entire northern hemisphere has experienced the maximum $^{14}CO_2$ concentration. The pattern in the southern hemisphere is similar, with the first maximum at the surface predicted in the subtropics after a few months. The entire southern hemisphere is reached by the first maximum within a year. Fig. 15, on the other hand, shows that the time of the overall highest concentrations is more than 1 year for most of the southern hemisphere. The higher concentrations of the 2nd year of the simulation, are due to transport of $^{14}CO_2$-rich air from the northern hemisphere. Within two years also remote parts of the southern hemisphere are reached by the peak in the $^{14}CO_2$ signal.

The absolute peak levels at tropopause levels in the northern hemisphere were observed already in January and April 1963 (Johnston, 1989) which is prior to the period simulated here. During the first years after this time a clear seasonal cycle has been found at some of the northern hemisphere surface stations (Nydal and Lövseth, 1996) (Fig. 16). Maximum concentrations are observed during summer indicating seasonal input from the

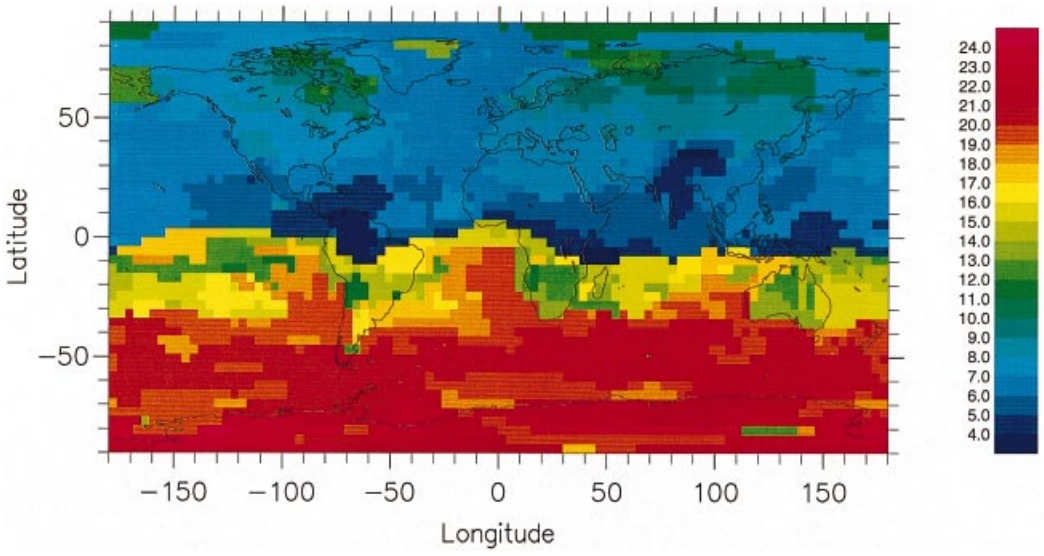

Fig. 15. Simulated time until the maximum concentration of $^{14}CO_2$ was reached at the surface. Unit: months.

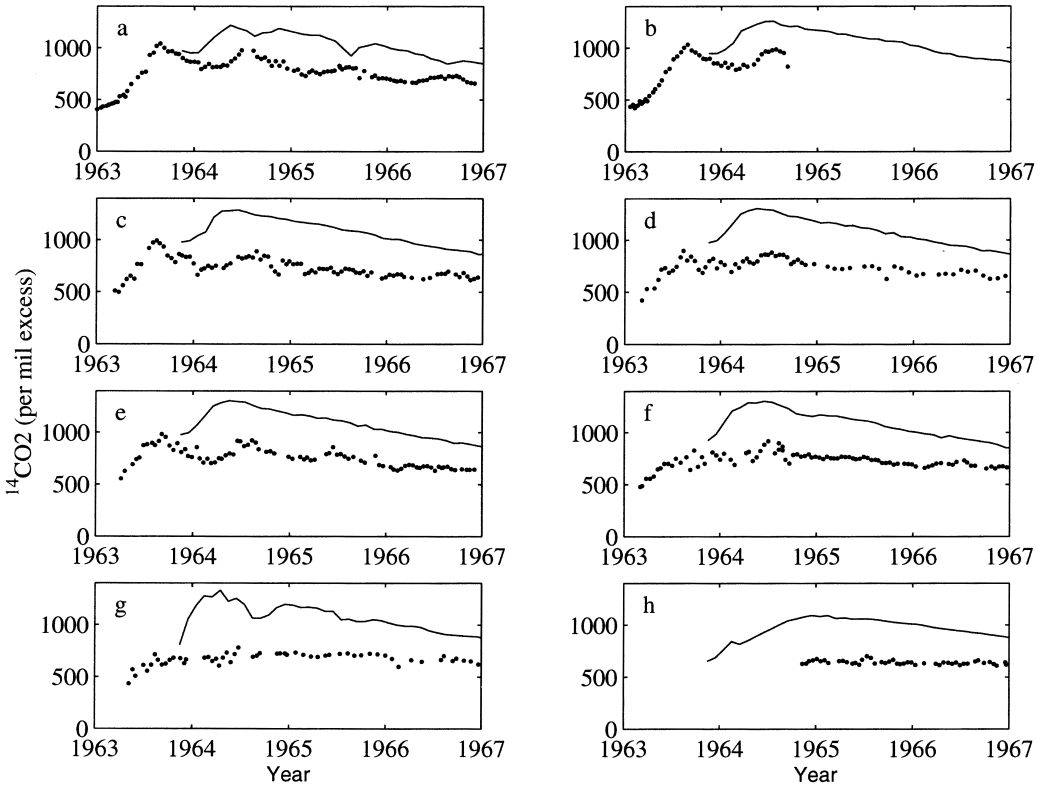

Fig. 16. Observed (dots) and simulated (full line) evolution of $^{14}CO_2$ at surface stations. The observations are from Nydal and Lövseth (1996): (a) Fruholmen, Norway (78°04N, 13°38E), (b) Lindesnes, Norway (57°59N, 07°04E), (c) Santiago de Compostela, Spain (42°53N, 08°26W), (d) Izana, Spain (28°N, 16°30W), (e) Mas Palomas, Spain (27°45N, 15°40W), (f) Dakar (1963–64) and Dakar-Fann (1964–68), Senegal (14°40N, 17°20W), (g) Debre Zeit, Ethiopia (8°40N, 38°58E) and (h) Fianarantsoa, Madagascar (21°27S, 47°05E). Unit: per mil excess relative to the NIST standard.

stratosphere of $^{14}CO_2$ (Nydal and Lövseth, 1983). The model simulated maxima, on the other hand, occur up to 4 months earlier than observed. This lead of the model before the observations indicates that the simulated downward transport is too fast. Further, the model overestimates the ground level $^{14}CO_2$ concentrations at the time of the maximum compared with the observed maximum. This overestimate, which is more pronounced at the stations located closer to the equator, also supports the notion of a too strong subtropical downward transport in the model. The lack of a clear seasonal cycle in the model results is probably due to the too rapid initial downward mixing of $^{14}CO_2$. Already after a few months of the simulation the tropospheric content of $^{14}CO_2$ is much higher than the stratospheric content (Fig. 4). The high tropospheric $^{14}CO_2$ content efficiently masks the seasonal signal from stratospheric downward transport in the subsequent years of the simulation. Fig. 16 also shows that the $^{14}CO_2$ concentrations decrease too rapidly at all observational stations. This rapid decrease indicates that the global sink terms are overestimated in the model, a feature also discussed by Hesshaimer et al. (1994).

4. Summary and conclusions

The ECHAM4 model is able to simulate the main features of the observed atmospheric SF_6 pattern, such as the vertical and latitudinal distribution in the troposphere and lowermost

stratosphere and the phase of the seasonal cycle at a remote observational site in the southern hemisphere. A comparison of the simulated vertical gradient of SF_6 in the tropopause region with observations shows that the model captures the stratospheric decline in mixing ratio with increasing altitude in the first 4 or 5 km above the tropopause. The ability of the model to predict the cross-tropopause gradient implies that the simulated upward net flux of SF_6 across the tropopause level is realistic.

The global stratospheric $^{14}CO_2$ content decreases rapidly at the beginning of the simulation. The calculated e-folding time during the first year is 1.3 years which is shorter than what has been deduced from observations indicating a too strong downward transport of $^{14}CO_2$. The model predicts maximum surface concentrations leading the observations with up to 4 months at low latitude sites in Africa and southernmost Europe. At high latitudes the simulated temporal evolution is in better agreement with observations both at the surface and in the free troposphere. Therefore, it is concluded that the overestimated downward transport of $^{14}CO_2$ is concentrated mainly to the subtropics.

The calculated interhemispheric exchange time of SF_6 of 0.9 years is slightly lower than previous estimates. This fact together with the too slow increase in the gradient between the hemispheres indicates that the interhemispheric transport in the troposphere is too strong. Also indicative of a too strong interhemispheric exchange is the too rapid buildup of stratospheric and tropospheric $^{14}CO_2$ compared with observations at 40°S.

It is clearly illustrated how the treatment of the upper boundary, with a strong damping and no transport across it, hampers a realistic simulation of tracer transport at the uppermost model levels. Especially above 20 km the mixing ratios of both SF_6 and $^{14}CO_2$ are underestimated with up to a factor 2 compared with a few measurements that are available at these levels. From a comparison with observations (Elkins et al., 1997) and previous simulations (Waugh et al., 1997) of the age of stratospheric air, it is concluded that the model simulates a too strong polewards transport of SF_6 in the southern hemisphere close to 20 km height.

5. Acknowledgements

The authors wants to thank Martin Heimann for providing emission data for SF_6. We are grateful to Bob Leifers who provided EML data and to Mannfred Maiss and Ingeborg Levin who provided correction factors for the EML data. Further we are grateful to Henning Rodhe, Eliza Manzini and Christine Land for constructive discussions and suggestions on the manuscript.

REFERENCES

Brinkop, S. and Sausen, R. 1997. A finite difference approximation for convective transports which maintains positive tracer concentrations. *Beitr. Phys. Atmosph.* **70**, 245–248.

Broecker, W., Peng, T.-H., Ostlund, G. and Stuiver, M. 1985. The distribution of bomb radiocarbon in the ocean. *J. Geophys. Res.* **90**, 6953–6970.

Crutzen, P. 1976. The possible importance of CSO for the sulfate layer of the stratosphere. *Geophys. Res. Lett.* **3**, 73–76.

DeMore, W. B., Sander, S. P., Golden, D. M., Hampson, R. F., Kurylo, M. J., Howard, C. J., Ravishankara, A. R., Kolb, C. E. and Molina, M. J. 1997. *Chemical kinetics and photochemical data for use in stratosphere modeling. Evaluation number 12.* JPL publication 97-4, Jet Propulsion Laboratory, Pasadena, Calif., USA.

Denning, A. S., Holzer, M., Gurney, K. R., Heimann, M., Law, R. M., Rayner, P. R., Fung, I. Y., Fan, S.-M., Taguchi, S., Friedlingstein, P., Balkanski, Y., Taylor, J., Maiss, M. and Levin, I. 1999. Three-dimensional transport and concentration of SF_6: a model intercomparison study (Transcom 2). *Tellus* **51**, 266–297.

Elkins, J. W., Fahey, D. W., Gilligan, J. M., Dutton, G. S., Baring, T. J., Volk, C. M., Dunn, R. E., Myers, R. C., Montzka, S. A., Wamsley, P. R., Hayden, A. H., Butler, J. H., Thompson, T. M., Swanson, T. H., Dlugokencky, E. J., Novelli, P. C., Hurst, D. F., Lobert, J. M., Ciciora, S. J., McLaughlin, R. J., Thompson, T. L., Winkler, R. H., Fraser, P. J., Steele, L. D. and Lucarelli, M. P. 1996. Airborne gas chromatograph for in situ measurements of long-lived species in the upper troposphere and lower stratosphere. *Geophys. Res. Lett.* **23**, 347–350.

Feichter, J. and Crutzen, P. J. 1990. Parameterization of vertical transport due to deep cumulus convection in a global transport model and its evaluation with ^{222}Radon measurements. *Tellus* **42**, 100–117.

Geller, L. S., Elkins, J. W., Lobert, J. M., Clarke, A. D., Hurst, D. F., Butler, J. H. and Myers, R. C. 1997. Tropospheric SF_6: observed latitudinal distribution

and trends, derived emissions and interhemispheric exchange time. *Geophys. Res. Lett.* **24**, 675–678.

Grewe, V. and Dameris, M. 1996. The large-scale mass-exchange between stratosphere and troposphere in the ECHAM3 model. In Staniforth, A. (ed.): *Research activities in atmospheric and oceanic modelling*. CAS/JSC working group on numerical experimentation. Report No. 23 WMO/TD No. 734.7.21–7.22, Geneva, Switzerland.

Hall, T. M. and Plumb, R. A. 1994. Age as a diagnostic of stratospheric transport. *J. Geophys. Res.* **99**, 1059–1070.

Harnisch, J., Borchers, R., Fabian, P. and Maiss, M. 1996. Tropospheric trends for CF_4 and C_2F_6 since 1982 derived from SF_6 dated stratospheric air. *Geophys. Res. Lett.* **23**, 1099–1102.

Hesshaimer, V., Heimann, M. and Levin, I. 1994. Radiocarbon evidence for a smaller oceanic carbon dioxide sink than previously believed. *Nature* **370**, 201–203.

Holton, J. R., Haynes, P. H., McIntyre, M. E., Douglas, A. R., Rood, R. B. and Pfister, L., 1995. Stratosphere–troposphere exchange. *Rev. Geophys.* **33**, 403–439.

Jacob, D. J., Prather, M. J., Wofsy, S. C. and McElroy, M. B. 1987. Atmospheric distribution of ^{85}Kr simulated with a general circulation model. *J. Geophys. Res.* **92**, 6614–6626.

Jacob, D. J., Prather, M. J., Rasch, P. J., Shia, R.-L., Balkanski, Y. J., Beagley, S. R., Bergmann, D. J., Blackshear, W. T., Brown, M., Chiba, M., Chipperfield, M. P., de Grandpré, J., Dignon, J. E., Feichter, J., Genthon, C., Grose, W. L., Kasibathla, P. S., Köhler, I., Kritz, M. A., Law, K., Penner, J. E., Ramonet, M., Reeves, C. E., Rotman, D. A., Stockwell, D. Z., van Velthoven, P. F. J., Verver, G., Wild, O., Yang, H. and Zimmermann, P. 1997. Evaluation and intercomparison of global atmospheric transport models using ^{222}Rn and other short-lived tracers. *J. Geophys. Res.* **102**, 5953–5970.

Johnston, H. 1989. Evaluation of excess carbon 14 and strontium 90 data for suitability to test two-dimensional stratospheric models. *J. Geophys. Res.* **94**, 18485–18493.

Kentarchos, A. S., Roelofs, G. J. and Lelieveld, J. 1999. Model study of a stratospheric intrusion event at lower midlatitudes associated with the development of a cutoff low. *J. Geophys. Res.* **104**, 1717–1727.

Kjellström, E. 1998. A three-dimensional global model study of carbonyl sulfide in the troposphere and the lower stratosphere. *J. Atmos. Chem.* **29**, 151–172.

Land, C. 1999. *Untersuchungen zum globalen Spurenstofftransport mit dem Atmosphaerenmodell ECHAM4.L39(DLR)*. PhD Thesis, University of Munich, Germany.

Leifer, R. 1992. *Project AIRSTREAM: Trace gas final report*. USDOE Report EML-549, New York, USA.

Levin, I. and Hesshaimer, V. 1996. Refining of atmospheric transport model entries by the globally observed passive tracer distributions of ^{85}Kr and sulfur hexafluoride (SF_6). *J. Geophys. Res.* **101**, 16745–16755.

Maiss, M. and Levin, I. 1994. Global increase of SF_6 observed in the atmosphere. *Geophys. Res. Lett.* **21**, 569–572.

Maiss, M., Steele, P., Francey, R. J., Fraser, P. J., Langenfelds, R. L., Trivett, N. B. A. and Levin, I. 1996. Sulfur hexafluoride — a powerful new atmospheric tracer. *Atmos. Environ.* **30**, 1621–1629.

Maiss, M. and Brenninkmeijer, C. A. M. 1998. Atmospheric SF_6 trends, sources and prospects. *Environ. Sci. Technol.* **32**, 3077–3086.

Nydal, R. and Lövseth, K. 1983. Tracing bomb ^{14}C in the atmosphere 1962–1980. *J. Geophys. Res.* **88**, 3621–3642.

Nydal, R. and Lövseth, K. 1996. *Carbon-14 measurements in atmospheric CO_2 from northern and southern hemisphere sites, 1962–1993*. ORNL/CDIAC-93, NDP-057. Carbon Dioxide information analysis center, Oak Ridge National Laboratory, Oak Ridge, Tennessee, USA, 67 pp.

Oeschger, H., Siegenthaler, U., Schotterer, U. and Gugelmann, A. 1975. A box diffusion model to study the carbon dioxide exchange in nature. *Tellus* **27**, 168–192.

Patra, P. K., Lal, S., Subbaraya, B. H., Jackman, C. H. and Rajaratnam, P. 1997. Observed vertical profile of sulphur hexafluoride (SF_6) and its atmospheric applications. *J. Geophys. Res.* **102**, 8855–8859.

Prather, M., McElroy, M., Wofsy, S., Russell, G. and Rind, D. 1987. Chemistry of the global troposphere: Fluorocarbons as tracers of air motions. *J. Geophys. Res.* **92**, 6579–6613.

Rasch, P. and Williamson, D. 1990. Computational aspects of moisture transport in global models of the atmosphere. *Q. J. R. Meteorol. Soc.* **116**, 1071–1090.

Ravishankara, A. R., Solomon, S., Turnipseed, A. A. and Warren, R. F. 1993. Atmospheric lifetimes of long-lived halogenated species. *Science* **259**, 194–199.

Roeckner, E., Arpe, K., Bengtsson, L., Christoph, M., Claussen, M., Dümenil, L., Esch, M., Giorgetta, M., Schlese, U. and Schulzweida, U. 1996. *The atmospheric general circulation model ECHAM-4: Model description and simulation of present-day climate*. Report no. 218, Max-Planck-Institute for Meteorology, Hamburg, Germany.

Roelofs, G. and Lelieveld, J. 1995. Distribution and budget of O_3 in the troposphere calculated with a chemistry general circulation model. *J. Geophys. Res.* **100**, 20983–20998.

Rosenlof, K. and Holton, J. 1993. Estimates of the stratospheric residual circulation using the downward control principle. *J. Geophys. Res.* **98**, 10465–10479.

Siegenthaler, U. 1983. Uptake of excess CO_2 by an outcrop-diffusion model of the ocean. *J. Geophys. Res.* **88**, 3599–3608.

Siegmund, P. C., van Velthoven, P. F. J. and Kelder, H., 1996. Cross-tropopause transport in the extratropical northern winter hemisphere diagnosed from high-

resolution ECMWF data. *Q. J. R. Meteorol. Soc.* **122**, 1921–1941.

Song, N., Starr, D., Wuebbles, D., Williams, A. and Larson, S. 1996. Volcanic aerosols and interannual variation of high clouds. *Geophys. Res. Lett.* **23**, 2657–2660.

Steil, B., Dameris, M., Brühl, C., Crutzen, P. J., Grewe, V., Ponater, M. and Sausen, R. 1997. Development of a chemistry module for GCMs: First results of a multi-annual integration. *Annales Geophysical* **16**, 205–228.

Stuiver, M. 1980. ^{14}C distribution in the Atlantic Ocean. *J. Geophys. Res.* **85**, 2711–2718.

Stuiver, M., Ostlund, H. G. and McConnaughey, T. A. 1981. GEOSECS Atlantic and Pacific ^{14}C distribution. In: *Carbon cycle modelling*, B. Bolin (ed.) John Wiley, New York, USA, pp. 201–221.

Telegadas, K. 1971. *The seasonal stratospheric distribution and inventory of carbon-14 from March 1955 to July 1969*. Health and Safety Lab, U.S. Atomic Energy Comm., Washington, DC, USA, Report 243.

Telegadas, K., Gray, J., Sowl, R. E. and Ashenfelter, T. E. 1972. *Carbon-14 measurements in the stratosphere from a balloon-borne molecular sieve sampler*, Health and Safety Lab., US Atomic Energy Comm., Washington, DC, USA, report 246.

Tiedtke, M. 1989. A comprehensive mass flux scheme for cumulus parameterization in large-scale models. *Mon. Wea. Rev.* **117**, 1779–1800.

Wang, Y., Jacob, D. J. and Logan, J. A. 1998. Global simulation of tropospheric O_3–NO_x–hydrocarbon chemistry (3). Origin of tropospheric O_3 and effects of nonmethane hydrocarbons. *J. Geophys. Res.* **103**, 10757–10767.

Waugh, D. W., Hall, T. M., Randel, W. J., Rasch, P. J., Boville, B. A., Boering, K. A., Wofsy, S. C., Daube, B. C., Elkins, J. W., Fahey, D. W., Dutton, G. S., Volk, C. M. and Vohralik, P. F. 1997. Three-dimensional simulations of long-lived tracers using winds from MACCM2. *J. Geophys. Res.* **102**, 21493–21513.

World Meteorological Organization (WMO). 1994. *Scientific assessment of ozone depletion*. Report 37, Global ozone research and monitoring project. Geneva, Switzerland.

World Meteorological Organization (WMO). 1986. *Atmospheric ozone 1985*: Report 16, *Global ozone research and monitoring project*. Geneva, Switzerland.